Artificial Cloud Seeding Using Liquid Carbon Dioxide: Comparisons of Experimental Data and Numerical Analyses

Seto, Jinichiro
Department of Earth and Ocean Sciences, National Defense Academy

Tomine, Kikuro
Department of Earth and Ocean Sciences, National Defense Academy

Wakimizu, Kenji
Faculty of Agriculture, Kyushu University

Nishiyama, Koji
Faculty of Engineering, Kyushu University

出版情報：Journal of Applied Meteorology and Climatology. 50 (7), pp.1417-1431, 2011-07-01. American Meteorological Society
バージョン：

Artificial Cloud Seeding Using Liquid Carbon Dioxide: Comparisons of Experimental Data and Numerical Analyses

JINICHIRO SETO AND KIKURO TOMINE

Department of Earth and Ocean Sciences, National Defense Academy, Yokosuka, Kanagawa, Japan

KENJI WAKIMIZU

Faculty of Agriculture, Kyushu University, Fukuoka City, Fukuoka, Japan

KOJI NISHIYAMA

Faculty of Engineering, Kyushu University, Fukuoka City, Fukuoka, Japan

(Manuscript received 23 June 2010, in final form 24 February 2011)

ABSTRACT

An artificial seeding experiment was carried out over the Genkai Sea, Japan, using liquid carbon dioxide. The seeded cloud was followed by an aircraft and radar at Kyushu University. A radar-echo intensity of 19 dB*Z* was formed in the seeded cloud where no radar echo was observed previously. The results of the experiment are analyzed using a numerical model [Weather Research and Forecasting Model (WRF), version 3.1] to evaluate the effects of the artificial seeding. The numerically simulated radar echo has a slightly stronger intensity and wider area than that observed. The results of the experiments were similar to those produced by the numerical model, however. Evaporation of cloud liquid water; growth of snow particles that is due to deposition, autoconversion, aggregation, and collection; and convection caused by released latent heat are shown in the numerical results as effects of the seeding experiment. The falling snow particles cause downward flow, which is compensated for by upward flow that causes the formation of new cloud liquid water as a secondary effect of seeding, although this secondary effect is confirmed only in the numerical results.

1. Introduction

For some time, glaciogenic cloud seeding has been proposed as an efficient technique for inducing artificial rainfall in supercooled clouds. The results of many such experiments have been varied, however. Enhancement of existing clouds accompanied by increases in precipitation has been reported in several case studies (e.g., English and Marwitz 1981) whereas others have reported decreased or no precipitation due to an increased number of ice particles (e.g., Hobbs and Politovich 1980). In addition, randomized experiments have been carried out with inconclusive results (e.g., Rangno and Hobbs 1995, 1997; Rosenfeld 1997; Dennis and Orville 1997; Bruintjes 1999; Silverman 2001; Garstang et al. 2004). Thus, many researchers have some doubt as to the efficiency of artificial seeding.

The above-mentioned studies that focused on demonstrating the efficiency of artificial seeding have involved statistical and physical analyses on an observational basis. One statistical method is to compare the results obtained in a randomized experiment from both artificially seeded and unseeded clouds over a long period in which large sample sizes can accumulate. Because there are numerous variations (cloud vertical and horizontal scales, cloud life, entrainment, etc.) among natural clouds even if the weather conditions are homogeneous in a seeding target region, however, it is difficult to obtain samples with an even distribution of storm intensities, that is, that are lacking bias in storms between seeded and nonseeded days. This is true unless experiments are conducted over a considerable number of years. For example, Gabriel and Rosenfeld (1990) reported an example of apparent bias in storms in a 6-yr experiment. Hobbs and Politovich (1980) found, however, that artificial seeding was effective

Corresponding author address: Kukiro Tomine, Earth and Ocean Sciences, National Defense Academy, Hashirimizu 1-10-20, Yokosuka, Kanagawa 239-8686, Japan.
E-mail: tomine@nda.ac.jp

DOI: 10.1175/2011JAMC2592.1

at producing precipitable-sized particles in nonprecipitating clouds and that the effects were relatively small when clouds were already precipitating. This finding suggests that nonprecipitating clouds would make a good target in cloud-seeding experiments, provided that cloud lifetime was long enough to support the growth of precipitation particles to sizes and densities that could reach the ground (Cooper and Lawson 1984).

Numerical models are also effective tools for comparison with observation-based analyses of experiments. Ice formation in mixed-phase cloud is minutely simulated by Fan et al. (2009). As examples of an artificial seeding simulation, Murakami et al. (2003) and Hashimoto et al. (2008) evaluated the seeding potential in the target region of the Echigo Mountains in Japan and reported that the amount of snowfall was expected to increase by 229 mm in total over two winters if cloud seeding were to be conducted under preferable conditions. Theses "preferable conditions" were determined by wind direction, wind speed, liquid water path, cloud water–weighted temperature, and the mass ratio of cloud water to total condensate water. Many unresolved problems currently remain with such investigations because of insufficient observations and the complicated processes in clouds, however.

A fundamental starting point for overcoming such complexity is 1) to obtain observationally unambiguous seeding results and 2) to compare the observations in the seeding experiment through the use of numerical cloud models. Here, we compare the significant features of a seeded region in a model with observations, made by both aircraft and onshore radar, of cloud that was seeded using liquid carbon dioxide.

Cloud seeding using liquid carbon dioxide was first numerically simulated by Guo et al. (2006). They compared cloud seeding using liquid carbon dioxide and silver iodide and found that liquid carbon dioxide was more effective than silver iodide for cloud seeding at atmospheric temperatures between 0° and −5°C. They had no observations to support these results, however. This study presented here is the first comparison of a real cloud-seeding experiment using liquid carbon dioxide with a numerical simulation.

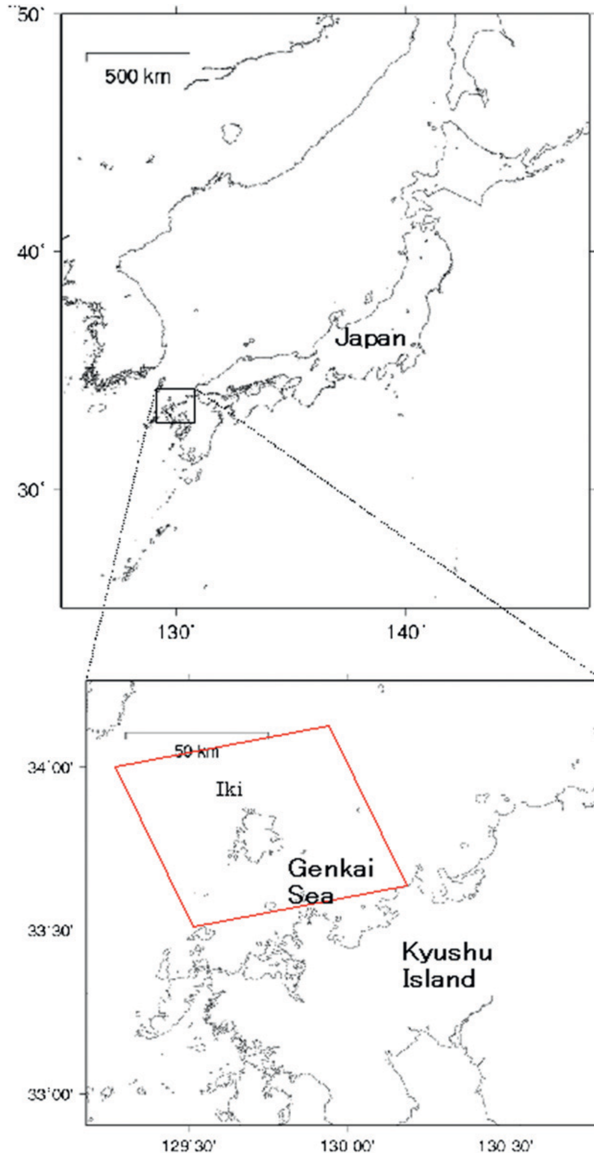

FIG. 1. Location of the artificial seeding experiment. The target area for the experiment is enclosed by the red quadrangle.

2. Seeding experiment

The seeding experiment was conducted over the Genkai Sea to the north of Kyushu Island, Japan, at 0917–0919 Japan standard time (JST) 4 February 2006 (Fig. 1).

a. General methods

The seeding experiment was carried out using an aircraft (P-3C; Kawasaki Heavy Industries, Ltd.) belonging to Air Development Squadron 51 of the Japan Maritime Self Defense Force. Liquid carbon dioxide has previously been used for homogeneous ice nucleation without the help of ice nuclei (Fukuta 1996) and was sprayed from a nozzle installed in a free-fall shooter under the tail. Liquid carbon dioxide evaporates rapidly to cool surrounding air to reach about −80°C when released into a standard atmosphere, and water vapor in the cooled air deposits instantaneously to generate 10^{13} of ice crystals per gram (Fukuta et al. 1971). Cloud droplets around the evaporating liquid carbon dioxide may freeze, but their number density is estimated to be negligible. The ice crystals can grow to at least 10 μm in radius by 30 s after generation (Fukuta and Takahashi

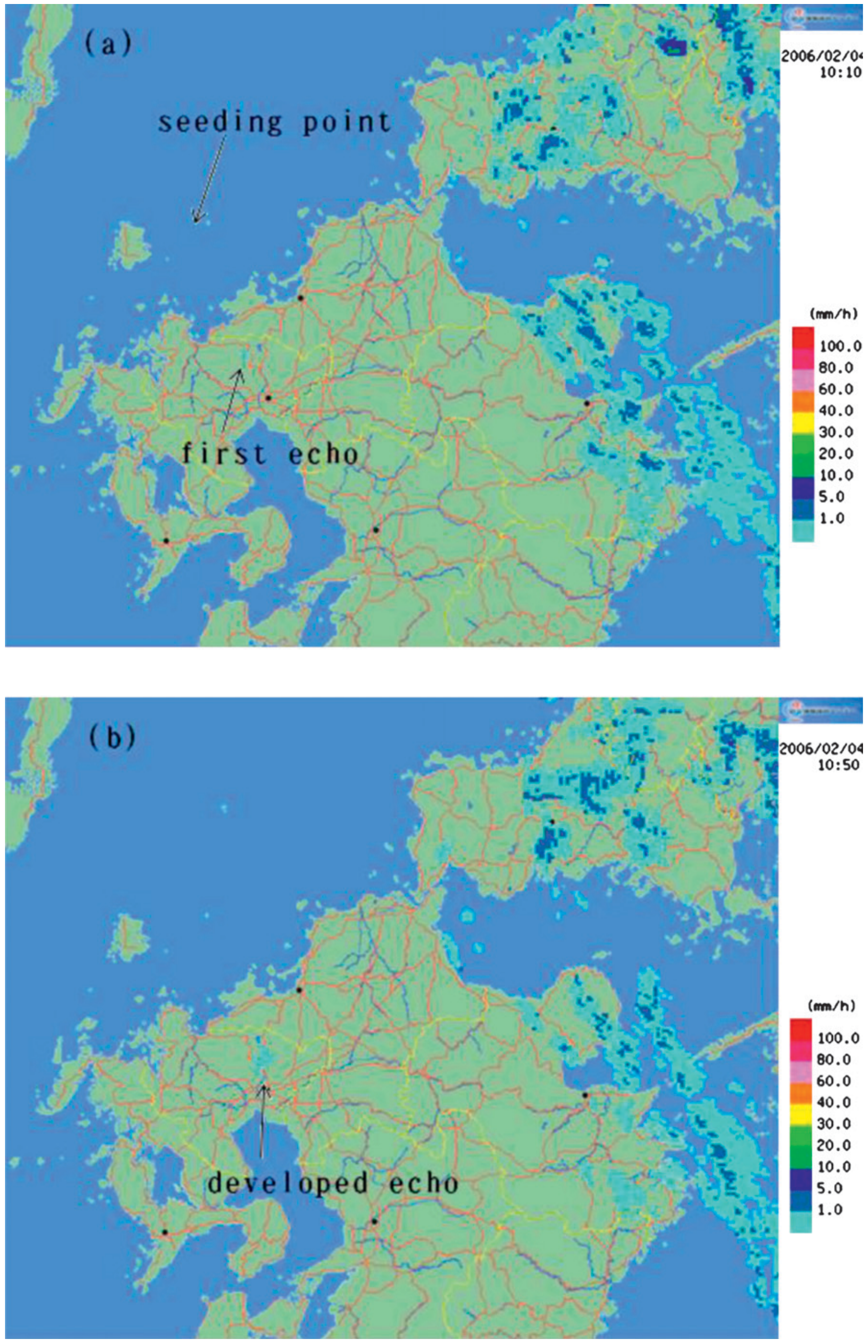

FIG. 2. Distribution of the radar echo at (a) 1010 and (b) 1050 JST 4 Feb 2006 (from the JMA).

1999). The seeding rate was 10 g s^{-1}, and the airspeed of the aircraft was 100 m s^{-1}, following Wakimizu et al. (2002). The seeding rate was chosen so as to generate a number of ice crystals that is adequate to change all of the liquid water in a cloud that has a 1 g kg^{-1} mixing ratio and that is 1 km in height and 4 km in width to droplets of 0.1 mm in radius. A wide radar echo had already passed eastward over the seeding area at 0820 JST, and there was no radar echo in the vicinity of the seeded area, except for over the east coast of Kyushu Island in the morning (Fig. 2a). Several stratocumuli were observed, and their cloud-top and cloud-bottom heights were about 2130 and 1070 m, respectively. Atmospheric temperatures were about −13° and −7.5°C at the cloud

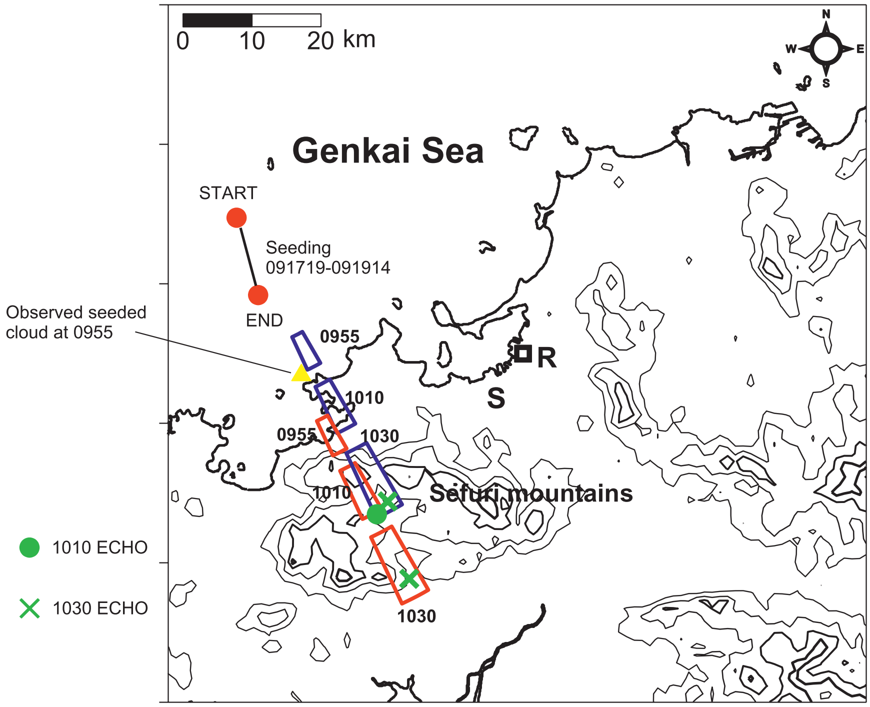

FIG. 3. Map showing the location of the seeding experiment and cloud characteristics during the seeding experiment. Locations of the seeding run (red circles), cloud location at 0955 JST (yellow triangle), radar echo at 1010 JST (green circle), and at 1030 JST (green cross) are shown. Trajectories of the points at the beginning and end of the seeding line in the cloud are shown as blue and red rectangles, respectively. The location of the radar at Kyushu University is indicated by the R. The location of the sounding observation (JMA) is indicated by the S.

top and bottom, respectively. Liquid carbon dioxide was sprayed inside one of the clouds at a height of 1372 m, where the atmospheric temperature was −9°C. Other information about the cloud, such as the liquid water content, cloud droplet concentration, and droplet spectra, unfortunately was not observed. The cloud was considered to be mainly formed of liquid water droplets and not of ice particles, because the brightness of the cloud was less than that of an ice cloud.

The seeding aircraft flew from the north-northwest to the south-southeast as it seeded the cloud with liquid carbon dioxide, as shown by the red circles in Fig. 3. The seeded cloud, which was transported south-southeastward, was monitored by the aircraft.

b. Results

It was confirmed that the cloud top had risen to 2220 m in an isothermal layer of −13°C by 0955 JST at the point indicated by the yellow triangle in Fig. 3, 38 min after the seeding. Other clouds around the seeded cloud looked to be suppressed in their development by the isothermal layer. The estimated trajectories of the points at the beginning and the end of the seeding line in the cloud are indicated in Fig. 3 by blue and red rectangles, respectively. To calculate the possible extent of the cloud trajectories, the wind speed and direction are assumed to be 17–22 kt (8.5–11 m s^{-1}) and 330°–335°, respectively, based on the middle level of the seeded cloud and profile of the upper wind at 0900 JST over the nearest observational point, which was 40 km away from the seeding line.

The X-band radar at Kyushu University, which is located at point R in Fig. 3, was then used for the analysis of the echo. At 1005 JST, a weak radar echo was first observed (Fig. 4a) on the southern edge of the trajectory of the cloud at the end of the seeding line (Fig. 3). This observation was about 50 min after the seeding experiment. This radar echo is the same as that shown as the first echo in Fig. 2a. The radar echo, which was observed near the Sefuri Mountains, had a horizontal scale of approximately 4 km, with a height and thickness of 2 and 1 km, respectively (Fig. 4c). No other radar echoes were observed in the vicinity of the radar echo at 1005 JST, and there were some radar echoes on the east coast of Kyushu Island in the distance. The radar echo studied in this paper developed to a maximum echo intensity of 19 dBZ, as shown in Figs. 4b and 4d at 1027 JST. These echoes were observed on the southern edges of the cloud trajectories at 1030 JST, which started

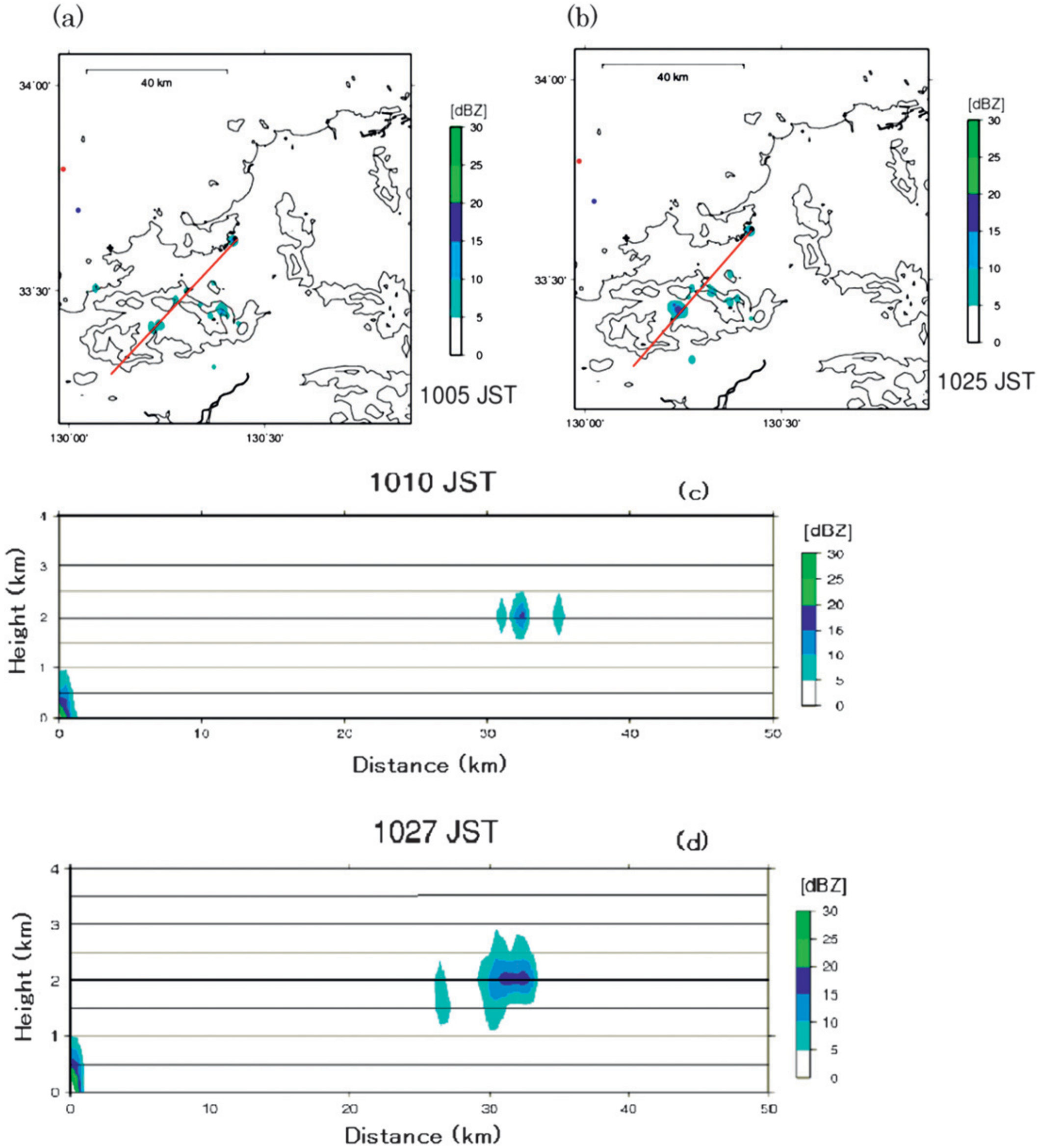

FIG. 4. Radar echo recorded at Kyushu University. Plan position indicator at (a) 1008 and (b) 1028 JST. Range–height indicator (RHI) at (c) 1010 and (d) 1027 JST. Red lines in (a) and (b) show the locations of the RHI.

from both ends of the seeding line (Fig. 3). The echoes then began to stretch downward, as shown in Fig. 4d, indicating the onset of precipitation. Because the echoes were hidden from the Kyushu University radar by the Sefuri Mountains after 1037 JST, their development was confirmed by the Japan Meteorological Agency (JMA) S-band radar (which is located at point S in Fig. 3) until 1050 JST, 90 min after the seeding experiment (Fig. 2b), and they dissipated at 1120 JST. A precipitation rate of less than 0.5 mm h^{-1} was recorded at 1115 JST at a station that was located under the radar echo. These findings imply that the radar echo was formed in the seeded cloud, because there was no radar echo in the vicinity of this echo, as shown in Fig. 2b, and it appeared on the cloud trajectories at the time at which the radar echoes were observed. Furthermore, it is likely that the radar echoes formed as a result of the seeding experiment because the period of 38 min taken for the clouds to rise after seeding agrees well with the observation by Wakimizu et al. (2002). They reported that a fluffy cloud came out from the original cloud top 44 min after the seeding and that the cloud top reached a maximum height 63 min after the seeding. Perhaps the duration of 50 min for the first appearance of the radar echo after

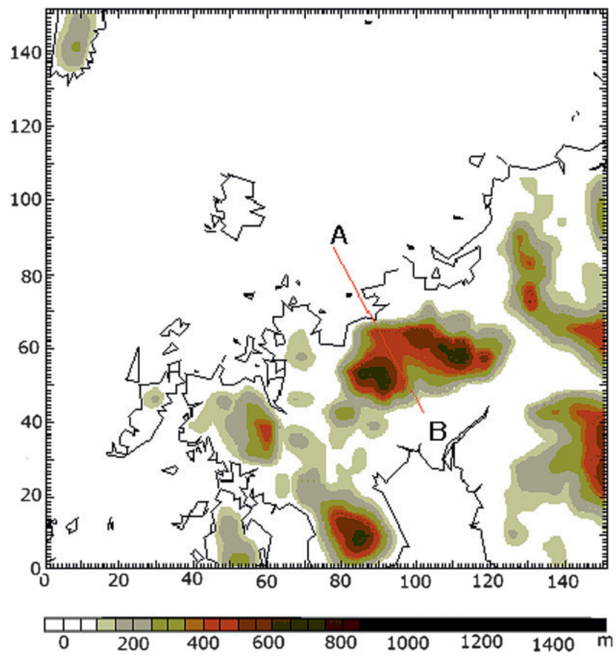

FIG. 5. The computational domain used in this study. Line AB represents the position of cross sections described hereinafter. The color-scale contour interval is 200 m.

the seeding may seem like a surprisingly long time. However, the ice concentration may have been high at first, and the ice crystals may have been subject to extreme competition, which would retard their growth, because the seeding rate of the liquid carbon dioxide was selected to form an adequate number density of ice particles once they diffused throughout the cloud, as described before.

3. Numerical experiment

a. Model description

A numerical experiment was undertaken to investigate the effects of the seeding experiment on the radar echo described above. The Weather Research and Forecasting Model (WRF), version 3.1, was used for the numerical analysis in this study. The model employs the Morrison double-moment scheme (Morrison et al. 2005, 2009) for the cloud microphysics, in which both the number concentration and mass mixing ratio of five hydrometeor species are predicted. The five hydrometeor species are cloud droplets, cloud ice, snow, rain, and graupel. The scheme is necessary to simulate cloud seeding using liquid carbon dioxide in this paper.

The model includes primary production (ice nucleation or droplet activation), condensation/deposition (evaporation/sublimation), autoconversion (parameterized transfer of mass and number concentration from the cloud ice and droplet classes to snow and rain through coalescence and diffusional growth), collection between hydrometeor species, melting/freezing, and ice multiplication (transfer of mass from the snow class to ice). The time tendency equations for graupel mixing ratio and number concentration are given by Reisner et al. (1998), except for the minimum mixing ratios for rain and snow required to produce graupel. An analytic approximation to the three-phase supersaturation equation that predicts the supersaturation field needed for the resolved droplet activation scheme is derived as shown in Morrison et al. (2005). The net grid-average condensation/deposition rate of cloud water and ice is given by the fractional cloud

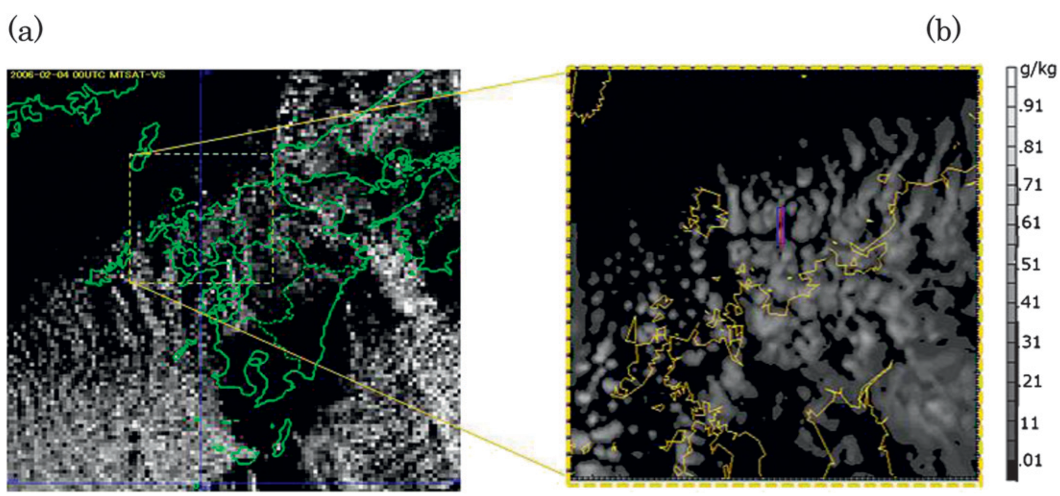

FIG. 6. Comparison of cloud. (a) Visible satellite image at 0900 JST 4 Feb 2006. The domain of the numerical simulation is shown by the yellow rectangle. (b) Numerically simulated cloud with a water mixing ratio of greater than 0.01 g kg^{-1} at the 850-hPa level. The color scale is shown at 0.05 g kg^{-1} intervals of the mixing ratio. The seeded area is shown by a blue rectangle with a purple line.

closure scheme of Zhang et al. (2003). Morrison and Gettelman (2008) modified the above scheme to include the Bergeron–Findeisen process, similar to the approach of Rotstayn et al. (2000).

The autoconversion of cloud ice to form snow is calculated by integration of the cloud ice mass- and number-weighted size distributions greater than a threshold size of 200 μm, following Ferrier (1994). Accretion of ice crystals by snow given by the continuous collection equation follows the method of Lin et al. (1983). The collection efficiency for collisions between cloud ice and snow is 0.1, following Reisner et al. (1998) and Murakami (1990). Self-collection of snow (or aggregation) follows Reisner et al. (1998), and self-collection of cloud ice is neglected. The autoconversion of cloud water to form rain is calculated by the Khairoutdinov and Kogan (2000) scheme.

Although it is desirable to predict the growth of each cloud ice particle with deposition to give the size distribution of the particles, the size distribution is represented by a gamma function in the model. This situation means that the simulated intensity of radar reflectivity or precipitation amount in the model may contain some uncertainty. The Yonsei University scheme and fifth-generation Pennsylvania State University–National Center for Atmospheric Research Mesoscale Model (MM5) similarity are adopted for the planetary boundary layer and the surface layer, respectively. The ‘‘Noah’’ land surface model is adopted. The Rapid Radiative Transfer Model scheme (Mlawer et al. 1997) and the Dudhia scheme (Hong et al. 2006) are adopted for longwave radiation and shortwave radiation, respectively.

The numerical simulation was performed for 12 h from 0300 to 1500 JST 4 February 2006. The initial and boundary conditions are formed from the objective analysis of National Centers for Environmental Prediction output and the mesoscale spectral model of the JMA. The computational domain consists of an outer area and an inner area. The outer area is set as 300 km × 300 km covered by a 3-km mesh, and the inner area covers 150 km × 150 km, with a 1-km mesh. The model has 40 vertical layers, and the top of the model is the 50-hPa level. The computational domain is shown in Fig. 5.

The computational domain is chosen to create the initial cloud adequately. We need the 300-km square domain and the 6-h time integral to generate the initial cloud before the seeding because the cloud is formed as a result of synoptic systems. It is very important to represent environmental conditions that are similar to those in the real experiment because this paper aims to analyze numerically the results of an actual artificial seeding experiment. In addition, Guo et al. (2006) used a numerical model with a 1-km mesh to investigate artificial seeding effects with silver iodide and liquid carbon dioxide. Hashino and Tripoli (2007) also used a 1-km-mesh bin model to describe the Spectral Ice Habit Prediction System (SHIPS). So we do not think that a 1-km grid spacing is unusually large to simulate the artificial seeding experiment qualitatively.

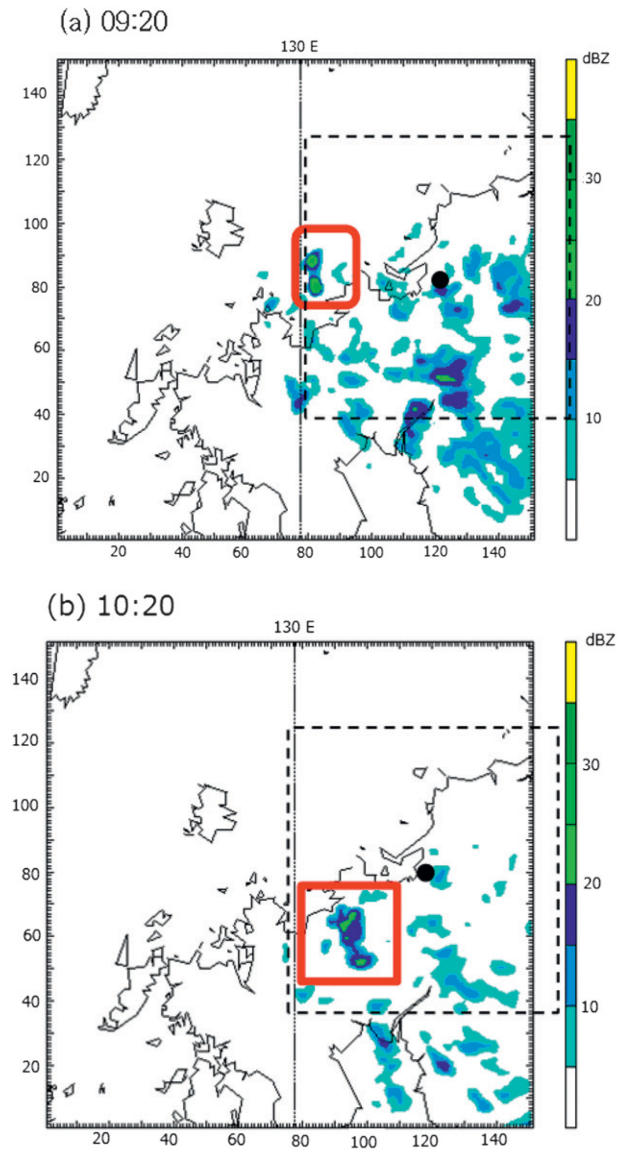

FIG. 7. Distributions of radar echo in the seeded cloud at the 850-hPa level at (a) 0920 and (b) 1020 JST 4 Feb 2006 (from JMA). The filled circle represents the position of the radar at Kyushu University.

It is true that Lin et al. (1983) simulated a thunderstorm in a two-dimensional model with a 19.2-km square domain and a 200-m grid interval to give the model a large amount of realism. Stevens et al. (1996) used a numerical model with 55-m horizontal spacing and 25-m

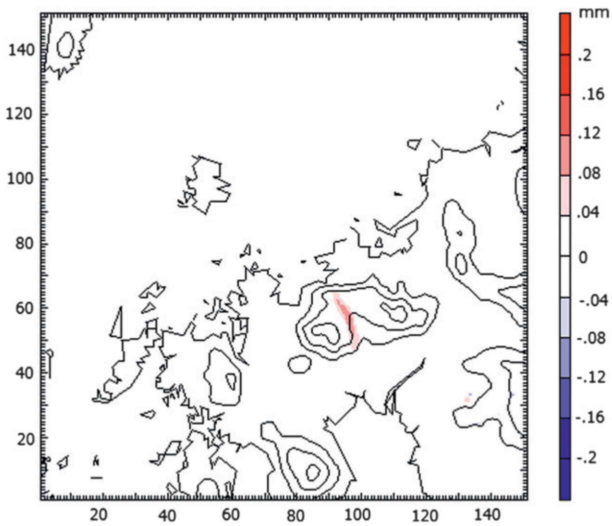

FIG. 8. Accumulated precipitation for 120 min between 0900 and 1100 JST from the seeded radar echo. The color-scale contour interval is 0.04 mm. The contour-line interval is 200 m.

vertical spacing to investigate the microphysical structure of stratocumulus and reported errors associated with limited vertical resolution. We think such a short grid interval is necessary to present results of the artificial seeding more quantitatively. In this paper, however, generation of the environmental conditions for the artificial seeding is more important than the quantitative representation for investigating the results of the real seeding experiment, because if the environmental conditions are inadequate then the numerical seeding experiment becomes meaningless. So we used the WRF model and can first analyze qualitatively the results of the real seeding experiment with liquid carbon dioxide.

The seeding experiment with liquid carbon dioxide is represented in the numerical simulation by increasing the mixing ratio and number density of cloud ice at 0900 JST in a rectangular parallelepiped domain, as shown in Fig. 6b. The actual seeding time around 0918 JST is not applied to the model run only for computational convenience. The real seeding experiment was carried out for 120 s with a seeding rate of 10 g s^{-1} at an aircraft speed of 100 m s^{-1}, giving a seeded domain 12 km long and a mass of seeded liquid carbon dioxide of 1200 g. The domain is set between 1511- and 1794-m height in the cloud, and the width was 1 km. The thickness and width of the domain are determined as the minimum allowable for the numerical model. The increased number density of cloud ice particles is 2.92×10^6 m^{-3} because 10^{13} of ice crystals will be generated per 1 g of liquid carbon dioxide (Fukuta et al. 1971), and they are assumed to spread uniformly over the domain of 1000 m (x direction) × 12 000 m (y direction) × 300 m (z direction).

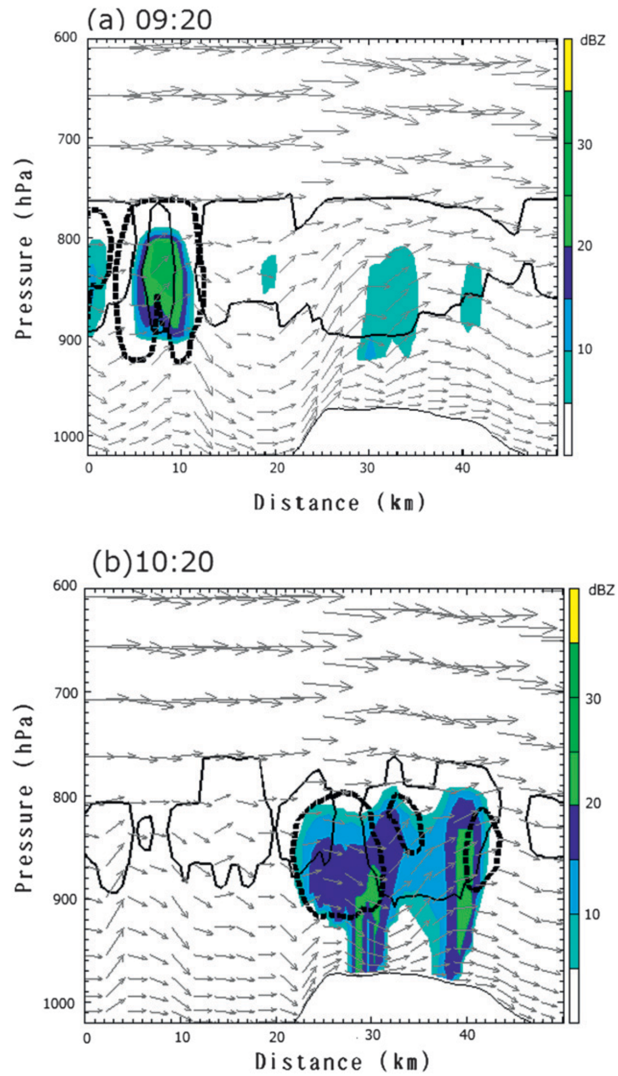

FIG. 9. Cross sections across the seeded radar echo at (a) 0920 and (b) 1020 JST. Solid and broken lines show areas of liquid water content of greater than 0.01 g kg^{-1} and cloud ice content of greater than 0.0005 g kg^{-1}, respectively. The configuration of the ground in (a) and (b) represents the Sefuri Mountains.

The mixing ratio of cloud ice is increased by 1.11×10^{-2} g kg^{-1}, assuming that the generated cloud ice particles grow rapidly into spheres of up to 10-μm radius. The average mixing ratio of cloud water and the number density of the cloud ice over the seeded domain are less than 3.8×10^{-1} g kg^{-1} and 1.47×10^2 kg^{-1}, respectively, before the seeding experiment. In nature, the concentration of ice crystals at −9°C is estimated to be between 20 and 300 m^{-3} (Meyers et al. 1992), and thus the simulated concentration of 1.47×10^2 kg^{-1} before the seeding experiment is adequate. The abrupt increase in the number density of the cloud ice particles is significant, but this is a characteristic of cloud seeding with liquid carbon

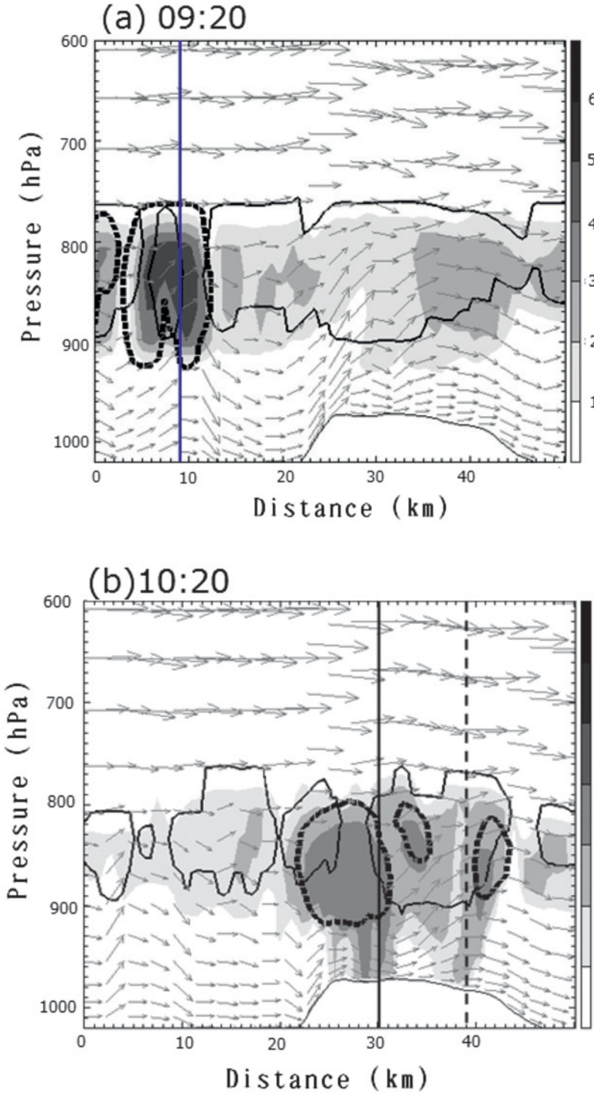

FIG. 10. Cross sections of the number density of snow particles in the seeded radar echo at (a) 0920 and (b) 1020 JST. The grayscale represents common logarithms of the number density (kg^{-1}) at intervals of unity. Vertical lines show the positions used to calculate the average mass profile of the snow particles.

dioxide. The increase in cloud water of 1.11×10^{-2} g kg^{-1} corresponds to only approximately 2.9% of the cloud water mixing ratio before the seeding experiment; this abrupt increase in the amount of cloud water is not natural, however. To compensate, we first decreased the amount of cloud water by 2.9% to conserve the amount of water in the cloud so as to investigate the influences of the increase in the amount of cloud water. The influence was found to be negligibly small, however, and therefore we decided to run the simulation without decreasing the amount of cloud water. Furthermore, we do not add aircraft-produced ice particles in the model, although

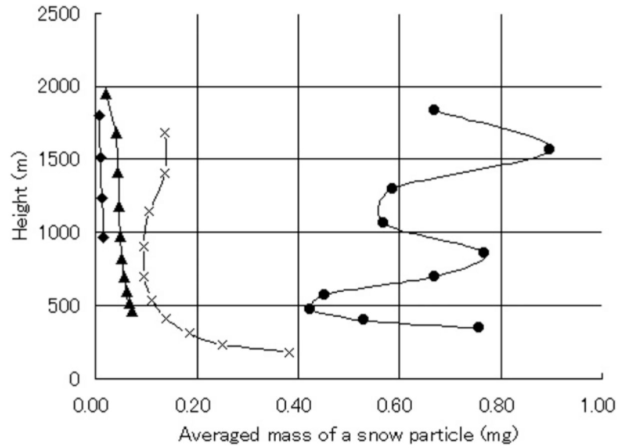

FIG. 11. Average mass profiles of a snow particle calculated for the lines in Fig. 10. Profiles at 0920 (Fig. 10a), 1020 (the front and back lines in Fig. 10b), and 1040 JST are represented by filled diamonds, filled circles, filled triangles, and times signs, respectively.

Rangno and Hobbs (1983, 1984) reported their presence. They reported that ice particles of 1100 L^{-1} were produced in a cylindrical-like volume along the flight track of the aircraft in a cloud of -8°C, and the diameter of the cylinder was about 300 m. In our numerical model, cloud seeding was simulated by the addition of a number density of 2.92×10^6 m^{-3} of cloud ice particles uniformly in the domain of 1000 m (x) × 12 000 m (y) × 300 m (z) as a result of the cloud seeding only, because the total number of cloud ice particles estimated from the cloud seeding (1.2×10^{16}) is far larger than the estimated total number of ice particles produced in the cylindrical-like volume of 300-m diameter and 12-km length along the flight track (9.3×10^{14}).

A comparison of the visible satellite image and numerically simulated cloud is shown in Fig. 6. The cloud distribution at the 850-hPa level is shown in Fig. 6b as a representative distribution because most of the cloud appeared in the lower atmosphere in the numerical simulation. The simulated cloud distribution over northern Kyushu Island and the Genkai Sea resembles that shown in the satellite image.

b. Results

Radar-echo intensity in the numerical model is represented as sum of the intensities determined by a gamma size distribution of five hydrometeor species (cloud droplets, cloud ice, rain, snow, and graupel) characterized by the intercept parameter, spectral index, and slope of the hydrometeor size distributions. A radar echo is formed in the seeded cloud at 0920 JST (Fig. 7a), 20 min after the seeding, at the 850-hPa level, and this radar echo does not appear in this position in the case

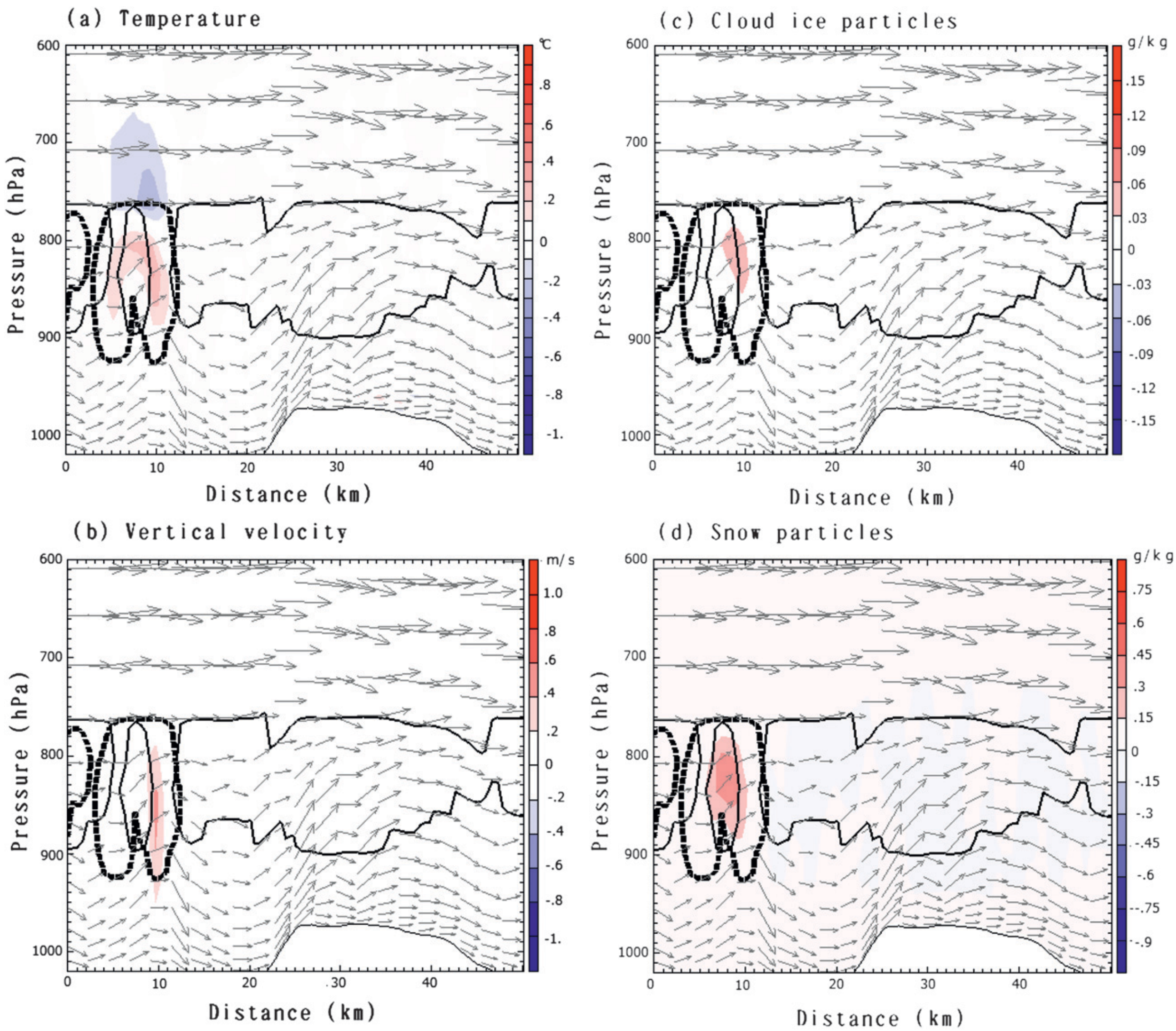

FIG. 12. Differences between the seeded and unseeded simulation cases in (a) atmospheric temperature, (b) vertical velocity, and the mixing ratios of (c) cloud ice particles, (d) snow particles, (e) total water content, (f) water vapor, and (g) liquid water at 0920 JST. The color-scale contour intervals are 0.1°C in (a), 0.2 m s^{-1} in (b), and 0.03, 0.15, 0.06, 0.03, and 0.15 g kg^{-1} in (c)–(g), respectively.

without seeding. Of course, some radar echo in the case without seeding is formed in other positions. The radar echo develops until 0950 JST, weakens gradually from 1020 JST (Fig. 7b) to 1040 JST, and then dissipates at 1050 JST. The distribution of simulated accumulated precipitation for 120 min between 0900 and 1100 JST is shown in Fig. 8. The maximum precipitation accumulation is 0.12 mm. The accumulated precipitation is formed along the path of the simulated seeded radar echo in the same location where the real seeded radar echo developed.

The cross sections of the radar echo shown in Fig. 9 lie along the path of the radar echo, as shown in Fig. 5. The seeded radar echo appears around the 850-hPa level on the left-hand side of Fig. 9a. It lies within a cloud layer (area of liquid water content higher than 0.01 g kg^{-1}). The cloud layer is between the 900- and 770-hPa levels where the temperatures are $-8°$ and $-14°$C, respectively. The mixing ratio of cloud ice is more than 0.0005 g kg^{-1} around the radar echo. Mountain waves are formed over the Sefuri Mountains, and the amplitude of the waves decreases with height, as shown in Fig. 9a, to show that the mountain waves are trapped near the ground. Atmospheric stratification is neutral below 2-km height at the time to allow formation of the trapped mountain waves. The rear part of the radar echo stretches to the ground surface on the windward side of the mountains but does not reach the ground at 0950 JST, when

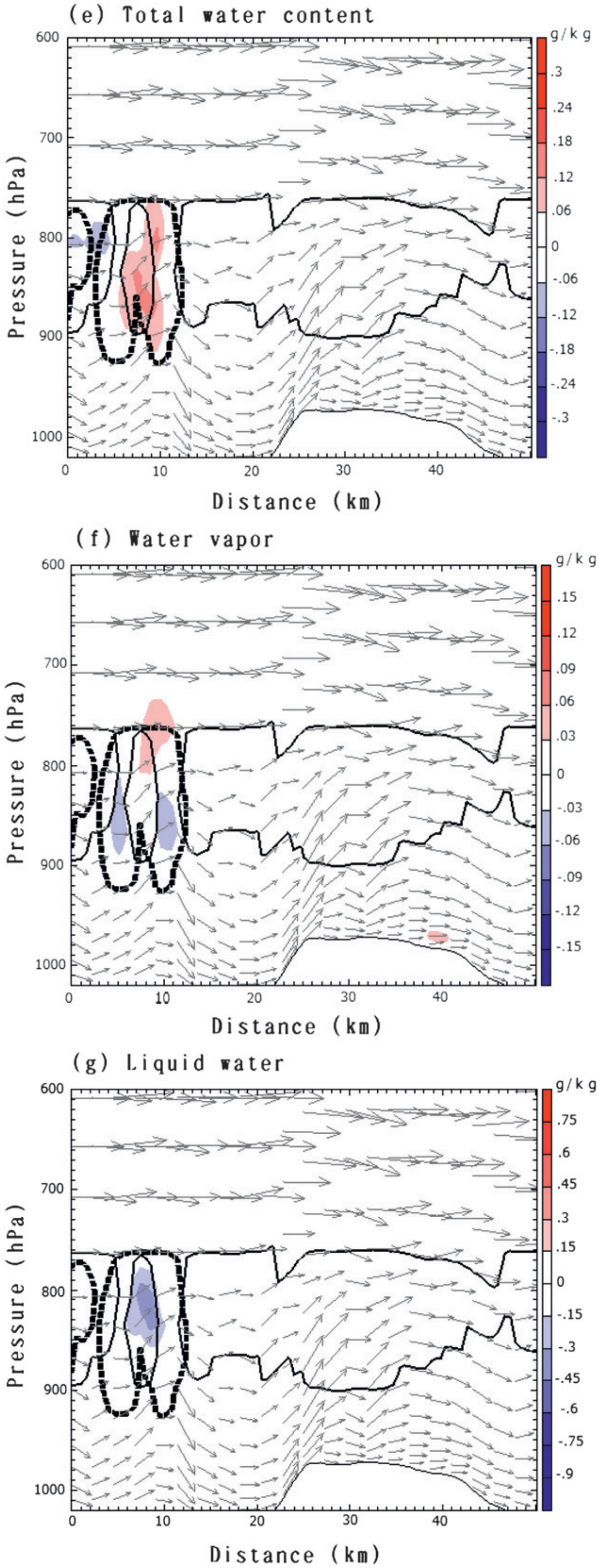

FIG. 12. (*Continued*)

the maximum radar-echo intensity is 28 dB*Z*. The radar echo stretches to the ground in the mountains at 1020 JST, and precipitation reaches the ground (Fig. 9b). With the developing radar echo, short waves of about 12-km length become predominant in the mountain waves over the Sefuri Mountains. The mountain waves are probably modified by the feature represented in the developing radar echo. The radar echo gradually weakens, and the precipitation area moves to the lee side of the mountains before dissipating at 1050 JST.

Cross sections of the number density of snow particles are shown in Fig. 10; these particles are the main reflectors of the above radar echo. In this model, a snow particle is defined to be larger than 200 μm in diameter and smaller particles are considered to be cloud ice. The dense (in number density) region of snow particles on the left-hand side of Fig. 10a corresponds to the seeded radar echo in Fig. 9a. This feature moves to the right and stretches to the ground surface in the seeded radar echo at 0950 JST. The number density is lower than that at 0920 JST. It decreases further over time, but the area with the highest concentration of snow particles reaches the ground surface at 1020 JST (Fig. 10b).

Average mass profiles of the snow particles calculated for the lines shown in Fig. 10 are presented in Fig. 11. These profiles represent the areas of the maximum echo intensity at the ground surface. The average mass at 0920 JST is small but increases significantly between 0920 and 1020 JST in the head of the seeded echo. Autoconversion from cloud ice, deposition, aggregation, and collection of cloud drops and ice contribute to snow particle growth, and the concentration of snow particles drastically decreases in the head echo (Figs. 10a and 10b). The profile in the head echo meanders irregularly at 1020 JST, because the line for calculation of the average mass passes through the edge of a high-concentration area. The average mass in the back echo is small at 1020 JST, before increasing at 1040 JST, especially near the ground surface. Snow particles begin to fall after they have grown sufficiently, and then the concentration decreases.

The cloud ice particles spread over a wide area between the 900- and 800-hPa levels by 0920 JST, as shown in Fig. 9a. Whether such fast diffusion of cloud ice particles formed from the liquid carbon dioxide sprayed from the aircraft occurs cannot be verified from the real seeding experiment. The fast diffusion may be a result of the method used to represent the seeding experiment in the numerical simulation, described further below. A strong radar echo similar to Fig. 9a appears in a simulation with seeding and without the mountain. The radar echo weakens when the mountain is not present, and no precipitation is simulated.

The calculated differences in several meteorological parameters between the seeded and unseeded cases are investigated to determine clearly the likely influence of the liquid carbon dioxide seeding with the mountain present. In the area of increased cloud ice particles, the differences in atmospheric temperature, vertical velocity, mixing ratio of cloud ice particles, snow particles, total water content, water vapor, and liquid water at 0920 JST are shown in Fig. 12. The broken line in Fig. 12c shows an area where the mixing ratio of cloud ice particles is larger than 0.0005 g kg^{-1}, as described in the caption of Fig. 9. An area with a mixing ratio of cloud ice particles exceeding 0.03 g kg^{-1} appears on the left-hand side of Fig. 12c. In the same area, temperature and vertical velocity increase (Figs. 12a,b), and temperature decreases above this area. The mixing ratio of snow particles and total water content increase (Figs. 12d,e), and water vapor and liquid water decrease in this area (Figs. 12f,g). The mixing ratio of water vapor increases above this area. These changes suggest the following processes are occurring: ice particles formed from the seeding diffuse in the area (Fig. 12c). Liquid water evaporates and decreases in mass (Fig. 12g), and water vapor deposition increases the mixing ratio of snow particles (Fig. 12d) and decreases the mixing ratio of water vapor (Fig. 12f). Latent heat of deposition is released, warming the area (Fig. 12a) and forming upward flow (Fig. 12b), which transports more moist air into the area to increase total water content (Fig. 12e). Most of the increase in total water content corresponds to an increase in snow particles. The upward flow in the cloud area deforms the wind above the cloud and causes a weak upward flow (Fig. 12b). The upward flow over the cloud area decreases temperature through adiabatic cooling and increases water vapor (Figs. 12a,f).

The radar echo reaches the surface (Fig. 9b) and precipitation starts to fall on the mountains at 1020 JST. The precipitation consists of snow particles (Fig. 10b), as described above. Furthermore, an increase in the area of liquid cloud water appears around the 830-hPa level between two moderate-echo areas (between 20 and 25 dB*Z*) over the mountains (Fig. 13a) where upward flow is formed (Fig. 13b). In the upward-flow area, the temperature falls below the 900-hPa level and warms above the 860-hPa level (Fig. 13c), showing that the upward flow is not caused by convection but instead occurs as compensation for the nearby downward flow. These two moderate-echo areas do not appear in the simulation without the mountain present and with seeding. Therefore, the development of the radar echoes and the precipitation over the mountain are considered to result from the artificial seeding associated with the upward flow on the windward side of the mountain.

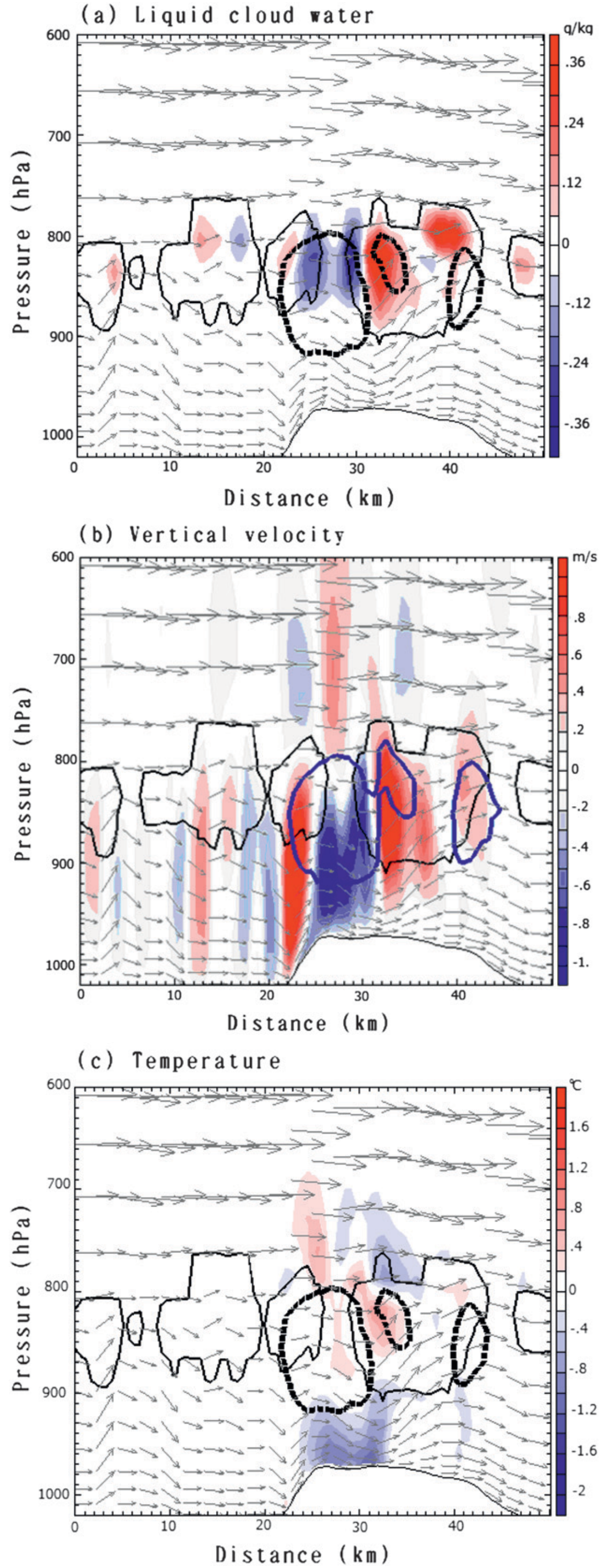

FIG. 13. As in Fig. 12, but for differences in (a) mixing ratio of liquid cloud water, (b) vertical velocity, and (c) temperature at 1020 JST. The color-scale contour intervals are 0.06 g kg^{-1} in (a), 0.1 m s^{-1} in (b), and 0.2°C in (c).

4. Discussion

The object of this study is the evaluation of a seeding experiment conducted and monitored by aircraft and a comparison with results obtained from a numerical model. A radar echo was formed as a result of seeding with liquid carbon dioxide on 4 February 2006. No radar echo was observed before the experiment at the cloud-seeding point, but some small radar echoes that dissipated within 5 min were observed over the Sefuri Mountains around the time of seeding. The radar echo associated with the seeding formed over the Sefuri Mountains 50 min after the release of the carbon dioxide (Fig. 2a), continued to develop for 90 min (Fig. 2b), and then dissipated 120 min after the time of seeding. A precipitation rate of less than 0.5 mm h^{-1} was recorded at a weather station under the radar echo. In the numerical experiment, no radar echo was formed in the case without seeding at the seeding point because the cloud particles of liquid water were too small and the concentration of large cloud ice particles was low. A small but clear radar echo was formed at the seeding point in the case with seeding, although it did not cause any precipitation without the mountain present. With seeding of the cloud in the model, a radar echo formed and intensified rapidly to a maximum echo intensity of 26 dBZ in the seeded cloud after 20 min (Fig. 7a).

The rapid intensification of the radar echo in the numerical experiment as compared with the much longer time in the actual experiment can be explained as follows. In the actual artificial seeding experiment, liquid carbon dioxide was sprayed from a nozzle positioned at the tail of an aircraft. The cloud ice particles formed by the liquid carbon dioxide were sprayed in a relatively fine line, so that the cloud ice particles would require a certain amount of time to diffuse in the cloud. On the other hand, in the numerical model, the seeding was represented as a homogeneous increase in the mixing ratio and number density of cloud ice particles in a domain of dimensions $12 \times 1 \times 0.3$ km^3, and it is expected that this method decreased the period required for diffusion through the cloud. The required period for diffusion throughout the domain of 1-km width from the seeded fine line is estimated to be about 55 min assuming that the distance of the turbulent diffusion transport is proportional to the square root of the time, because aircraft-produced ice particles took 5 min to spread into a cylindrical-like volume 300 m in diameter (Rangno and Hobbs 1983).

The simulated radar echo developed for 50 min, maintained an intensity of 26 dBZ for 30 min after its development (Fig. 7b), and dissipated 110 min after the time of seeding in the numerical model. The real radar echo developed for 90 min and dissipated 120 min after the seeding. Therefore, the time evolution of the real experiment is similar to that of the numerical simulation except for the time of onset of the initial radar echo. Furthermore, accumulated precipitation of 0.12 mm is numerically represented over the Sefuri Mountains (Fig. 8) in the position where the real radar echo was intensified. The accumulated precipitation amount of 0.12 mm corresponds to a precipitation rate of 0.24 mm h^{-1} because the radar echo passed over the mountain over a period of 30 min, and real precipitation weaker than 0.5 mm h^{-1} was recorded below the seeded cloud by the rain gauge of the Automated Meteorological Data Acquisition System (AMeDAS).

Other similarities between the numerical model and the real experiment are described as follows. The radar echo appeared to be roughly between a height of 1.5 and 2.5 km in the real experiment (Figs. 4b and 4d) and between 1 and 2 km (Fig. 9a) in the numerical simulation. The horizontal position and direction of the radar-echo movement were similar in each case. The speed of the movement was 8.5–11 m s^{-1} in the real experiment and slightly lower at 8 m s^{-1} in the numerical simulation. The real maximum radar-echo intensity was 19 dBZ after 70 min (Fig. 4d), whereas it was 26 dBZ after 50 min in the simulation. So the radar-echo intensity is overestimated in the numerical model. The overestimation may be attributable to differences of the initial liquid water content in the seeded cloud between the real and the simulated experiments, the assumption of the drop size distribution being represented by a gamma function in the model, and grid spacing that was insufficient to resolve the seeded cloud.

To understand the processes that formed the real radar echo in this study, the seeding experiment was simulated numerically. The results of the numerical modeling indicate that ice particles formed from the artificial seeding diffused in the area (Fig. 12c) 20 min after seeding. Liquid water then evaporated and decreased (Fig. 12g). Water vapor deposition increased the mixing ratio of snow particles (Fig. 12d) and hence decreased water vapor mixing ratio (Fig. 12f). The latent heat derived from deposition was released, warming the area (Fig. 12a). The warmed air formed an updraft (Fig. 12b), which transported more moist air into the area to increase the total water content (Fig. 12e). Most of the increase in total water content corresponded to an increase in snow particles. The updraft also decreased temperature and increased water vapor content just above the area of high concentration of cloud ice, transporting humid air upward adiabatically (Figs. 12a,f). The snow particles then grew in the upward flow on the windward side of the mountain and fell as precipitation on the mountains (Figs. 10b, 11). The Wegener–Bergeron–Findeisen (WBF) process, in which ice crystals grow with decreasing liquid water drops, seems to works in the simulations, because the mixing ratio of snow particles increases and that of liquid water decreases with the artificial seeding as shown in Figs. 12d and 12g. It is shown by Korolev (2007) that the WBF mechanism works only under a limited range of conditions. In this case $N_i r_i$ is about 30 μm cm^{-3} and the vertical velocity is between 0 and 60 cm s^{-1} at the initial period of the seeding to fulfill the conditions necessary for the mechanism to work, where N_i and r_i are the number concentration and mean radius of ice particles, respectively. Then, the above-described processes in the artificial seeding strongly suggest that the radar echo in the real experiment was formed as a result of the artificial seeding.

Furthermore, the upward flow in the numerical model likely formed to compensate for the downward flow brought about by the precipitation (Fig. 13b). In the upper parts of the adjacent upward flow, an increased area of liquid cloud water appeared between two moderate-echo areas (between 20 and 25 dBZ) over the mountains (Fig. 13a).

Ice crystals generated through evaporation of liquid carbon dioxide are supposed to spread throughout a cylindrical-like volume of 300-m diameter in the real atmosphere. In this study, a horizontal grid spacing of 1 km and a vertical grid size of 300 m were utilized to generate the initial clouds and meteorological conditions for the seeding experiment as described before. Therefore, the initial diffusion process of the ice crystals within the cylindrical-like volume cannot be evaluated using this model. Moreover, the radar-echo intensity seems to be overestimated as described before. Therefore it is questionable whether the grid spacing is adequate to resolve the seeded cloud. For example, the 25-dBZ radar-echo areas in Fig. 9c are only 1 or 2 km wide. The whole radar-echo areas are about 5 km wide and 1 km thick above the mountain surface, however, and the wavelength of mountain waves is modified by the radar echo (or by the seeded clouds) to be 12 km, as described before. Therefore, the horizontal scale of the dynamical system of the seeded clouds is estimated to be about 12 km. In a general way, the 1-km grid spacing is considered to be adequate to simulate cloud systems of 12-km horizontal scale, although the maximum radar-echo intensity and minute structure of the radar echo cannot be resolved well.

5. Conclusions

In this study, an isolated radar echo that appeared following an artificial seeding experiment over northern Kyushu Island in Japan on 6 February 2006 is simulated well by a sophisticated numerical model and is compared with unseeded clouds in the region. The model results support the conclusion that this isolated radar echo was the result of seeding in association with the presence of the mountain. In addition, the model calculations suggest that liquid cloud water was enhanced by an updraft adjacent to the seeded region that compensated for downdrafts brought about by precipitation in the seeded area.

Acknowledgments. We express great gratitude to Prof. N. Fukuta for his continuous encouragement to study artificial cloud seeding and for his invaluable advice.

REFERENCES

Bruintjes, R. T., 1999: A review of cloud seeding experiments to enhance precipitation and some new prospects. *Bull. Amer. Meteor. Soc.,* **80,** 805–820.

Cooper, W. A., and R. P. Lawson, 1984: Physical interpretation of results from the HIPLEX-1 experiment. *J. Climate Appl. Meteor.,* **23,** 523–540.

Dennis, A. S., and H. D. Orville, 1997: Comments on "A new look at the Israeli cloud seeding experiments." *J. Appl. Meteor.,* **36,** 277–278.

English, M., and J. D. Marwitz, 1981: A comparison of AgI and CO_2 seeding effects in Alberta cumulus clouds. *J. Appl. Meteor.,* **20,** 483–495.

Fan, J., M. Ovtchinnikov, J. M. Comstock, S. A. McFarlane, and A. Khain, 2009: Ice formation in Arctic mixed-phase clouds: Insights from a 3-D cloud resolving model with size resolved aerosol and cloud microphysics. *J. Geophys. Res.,* **114,** D04205, doi:10.1029/2008JD010782.

Ferrier, B., 1994: A double-moment multiple-phase four-class bulk ice scheme. Part I: Description. *J. Atmos. Sci.,* **51,** 249–280.

Fukuta, N., 1996: Low-level penetration seeding with homogeneous ice nucleant for optimization of the induced microphysics–dynamics interactions. Preprints, *13th Conf. on Planned and Inadvertent Weather Modification,* Atlanta, GA, Amer. Meteor. Soc., 164–171.

——, and T. Takahashi, 1999: The growth of atmospheric ice crystals: A summary of findings in vertical supercooled cloud tunnel studies. *J. Atmos. Sci.,* **56,** 1963–1979.

——, W. A. Schmeling, and L. F. Evans, 1971: Experimental determination of ice nucleation by falling dry ice pellets. *J. Appl. Meteor.,* **10,** 1174–1179.

Gabriel, K. R., and D. Rosenfeld, 1990: The second Israeli rainfall stimulation experiment: Analysis of precipitation on both targets. *J. Appl. Meteor.,* **29,** 1055–1067.

Garstang, M., R. Bruintjes, R. Serafin, H. Orville, B. Boe, W. Cotton, and J. Warburton, 2004: Weather modification: Finding common ground. *Bull. Amer. Meteor. Soc.,* **85,** 647–655.

Guo, X., X. G. Zheng, and D. Jin, 2006: A numerical comparison study of cloud seeding by silver iodide and liquid carbon dioxide. *Atmos. Res.,* **79,** 183–226.

Hashimoto, A., T. Kato, S. Hayashi, and M. Murakami, 2008: Seedability assessment for winter orographic snow clouds over the Echigo Mountains. *SOLA,* **4.** [Available online at http://www.jstage.jst.go.jp/article/sola/4/0/69/_pdf.]

Hashino, T., and G. J. Tripoli, 2007: The Spectral Ice Habit Prediction System (SHIPS). Part I: Model description and simulation of the vapor deposition process. *J. Atmos. Sci.,* **64,** 2210–2237.

Hobbs, P. V., and M. K. Politovich, 1980: The structures of summer convective clouds in eastern Montana. II: Effects of artificial seeding. *J. Appl. Meteor.,* **19,** 664–675.

Hong, S. Y., Y. Noh, and J. Dudhia, 2006: A new vertical diffusion package with an explicit treatment of entrainment processes. *Mon. Wea. Rev.,* **134,** 2318–2341.

Khairoutdinov, M. F., and Y. Kogan, 2000: A new cloud physics parameterization in a large-eddy simulation model of marine stratocumulus. *Mon. Wea. Rev.,* **128,** 229–243.

Korolev, A., 2007: Limitations of the Wegener–Bergeron–Findeisen mechanism in the evolution of mixed-phase clouds. *J. Atmos. Sci.,* **64,** 3372–3375.

Lin, Y.-L., R. D. Farley, and H. D. Orville, 1983: Bulk parameterization of the snow field in a cloud model. *J. Appl. Meteor.,* **22,** 1065–1089.

Meyers, M. P., P. J. Demott, and W. R. Cotton, 1992: New primary ice-nucleation parameterizations in an explicit cloud model. *J. Appl. Meteor.,* **31,** 708–721.

Mlawer, E. J., S. J. Taubman, P. D. Brown, M. J. Iacono, and S. A. Clough, 1997: Radiative transfer for inhomogeneous atmosphere: RRTM, a validated correlated-*k* model for the long wave. *J. Geophys. Res.,* **102,** 16 663–16 682.

Morrison, H., and A. Gettelman, 2008: A new two-moment bulk stratiform cloud microphysics scheme in the Community Atmospheric Model, version 3 (CAM3). Part I: Description and numerical tests. *J. Climate,* **21,** 3642–3659.

——, J. A. Curry, and V. I. Khvorostyanov, 2005: A new double-moment microphysics parameterization for application in cloud and climate models. Part I: Description. *J. Atmos. Sci.,* **62,** 1665–1677.

——, G. Thompson, and V. Tatarskii, 2009: Impact of cloud microphysics on the development of trailing stratiform precipitation in a simulated squall line: Comparison of one- and two-moment schemes. *Mon. Wea. Rev.,* **137,** 991–1007.

Murakami, M., 1990: Numerical modeling of dynamical and microphysical evolution of an isolated convective cloud—The 19 July 1981 CCOPE cloud. *J. Meteor. Soc. Japan,* **68,** 107–128.

——, N. Orikasa, M. Hoshimoto, K. Kusunoki, H. Kosuge, and H. Ikeda, 2003: Present state of Japanese research on orographic snow cloud modification for water resources augmentation. *Proc. Eighth Scientific Conf. on Weather Modification,* Casablanca, Morocco (WMO TD 1146), 95–98.

Rangno, A. L., and P. V. Hobbs, 1983: Production of ice particles in clouds due to aircraft penetration. *J. Appl. Meteor.,* **22,** 214–232.

——, and ——, 1984: Further observations of the production of ice particles in clouds by aircraft. *J. Appl. Meteor.,* **23,** 985–987.

——, and ——, 1995: A new look at the Israeli cloud seeding experiments. *J. Appl. Meteor.,* **34,** 1169–1193.

——, and ——, 1997: Reply. *J. Appl. Meteor.,* **36,** 279.

Reisner, J., R. M. Rasmussen, and R. T. Bruintjes, 1998: Explicit forecasting of supercooled liquid water in winter storms using the MM5 mesoscale model. *Quart. J. Roy. Meteor. Soc.,* **124,** 1071–1107.

Rosenfeld, D., 1997: Comments on "A new look at the Israeli cloud seeding experiments." *J. Appl. Meteor.,* **36,** 260–271.

Rotstayn, L. D., B. F. Ryan, and J. J. Katzfey, 2000: A scheme for calculation of the liquid fraction in mixed-phase stratiform clouds in large-scale models. *Mon. Wea. Rev.,* **128,** 1070–1088.

Silverman, B. A., 2001: A critical assessment of glaciogenic seeding of convective clouds for rainfall enhancement. *Bull. Amer. Meteor. Soc.,* **82,** 903–923.

Stevens, B., G. Feingold, W. R. Cotton, and R. L. Walko, 1996: Elements of the microphysical structure of numerically simulated nonprecipitating stratocumulus. *J. Atmos. Sci.,* **53,** 980–1006.

Wakimizu, K., and Coauthors, 2002: A low-level penetration seeding experiment of liquid carbon dioxide in a convective cloud. *Hydrol. Processes,* **16,** 2239–2253.

Zhang, M., W. Lin, C. S. Bretherton, J. J. Hack, and P. J. Rasch, 2003: A modified formulation of fractional stratiform condensation rate in the NCAR Community Atmosphere Model (CAM2). *J. Geophys. Res.,* **108,** 4035, doi:10.1029/2002JD002523.